

# JGR Space Physics

## RESEARCH ARTICLE

10.1029/2021JA029109

### Special Section:

Geospace multi-point observations in Van Allen Probes and Arase era

### Key Points:

- Ring current Atmosphere interactions Model with Self Consistent magnetic field (RAM-SCB) reproduced the particle fluxes very well observed by Arase satellite in inner magnetosphere during November 2017 magnetic storm
- The ring current pressure distribution from RAM-SCB in inner magnetosphere shows agreement with ground magnetic data
- The electron pressure contributed ~18% to the dawn-side ground magnetic depression after substorm injections

### Correspondence to:















S. Kumar,  
[sandeepk.iig@gmail.com](mailto:sandeepk.iig@gmail.com)

### Citation:

Kumar, S., Miyoshi, Y., Jordanova, V. K., Engel, M., Asamura, K., Yokota, S., et al. (2021). Contribution of electron pressure to ring current and ground magnetic depression using RAM-SCB simulations and Arase observations during 7–8 November 2017 magnetic storm. *Journal of Geophysical Research: Space Physics*, 126, e2021JA029109. <https://doi.org/10.1029/2021JA029109>

Received 11 JAN 2021  
 Accepted 24 MAY 2021

## Contribution of Electron Pressure to Ring Current and Ground Magnetic Depression Using RAM-SCB Simulations and Arase Observations During 7–8 November 2017 Magnetic Storm

S. Kumar<sup>1</sup> , Y. Miyoshi<sup>1</sup> , V. K. Jordanova<sup>2</sup> , M. Engel<sup>2</sup> , K. Asamura<sup>3</sup> , S. Yokota<sup>4</sup> , S. Kasahara<sup>5</sup> , Y. Kazama<sup>6</sup> , S.-Y. Wang<sup>6</sup> , T. Mitani<sup>3</sup> , K. Keika<sup>5</sup> , T. Hori<sup>1</sup> , C. Jun<sup>1</sup> , and I. Shinohara<sup>3</sup> 

<sup>1</sup>Institute for Space-Earth Environmental Research, Nagoya University, Nagoya, Japan, <sup>2</sup>Space Science and Application, Los Alamos National Laboratory, Los Alamos, NM, USA, <sup>3</sup>ISAS/JAXA, Sagami-hara, Japan, <sup>4</sup>Osaka University, Toyonaka, Japan, <sup>5</sup>University of Tokyo, Tokyo, Japan, <sup>6</sup>ASIAA, Taipei, Taiwan

**Abstract** Understanding the physical processes that control the dynamics of energetic particles in the inner magnetosphere is important for both space-borne and ground-based assets essential to the modern society. The storm time distribution of ring current particles in the inner magnetosphere depends strongly on their transport in the evolving electric and magnetic fields along with particle acceleration and loss. In this study, we investigated the ring current particle variations using observations and simulations. We compared the ion ( $H^+$ ,  $He^+$ , and  $O^+$ ) and electron flux and plasma pressure variations from Arase observations with the self-consistent inner magnetosphere model: Ring current Atmosphere interactions Model with Self Consistent magnetic field (RAM-SCB) during the 7–8 November 2017 geomagnetic storm. We investigated the contribution of the different species (ions and electrons) to the magnetic field deformation observed at ground magnetic stations ( $09^\circ$ – $45^\circ$  MLat) using RAM-SCB simulations. The results show that the ions are the major contributor with ~88% and electrons contribute ~12% to the total ring current pressure. It is also found that the electron contribution is non-negligible (~18%) to the ring current in dawn-side during the main phase of the storm. Thus, the electron contribution to the storm time ring current is important and should not be neglected.

## 1. Introduction

There is increased interest recently in understanding Sun-Earth interactions and space weather events due to the increasing reliability on space-based technological systems. Geomagnetic storms are among the most important phenomenon of space weather effects on Earth. Intense geomagnetic storms can cause severe damage to satellites, communications and power transmission lines (Jordanova et al., 2020 and references therein). The southward interplanetary magnetic field (IMF)  $B_z$  in solar wind allows magnetic reconnection with geomagnetic field which transfer energy from the solar wind to the Earth's magnetosphere (Dungey, 1961; Gonzalez et al., 1994). The ring current is a near-equatorial westward electric current flowing toroidally around the Earth ( $\sim 2$ – $7 R_E$ ), formed by charged particle (a few kilo-electronvolts to a few hundred of kilo-electronvolts) pressure gradients and drift motion (Daglis et al., 1993, 1999; Ebihara & Miyoshi, 2011; Frank, 1967; Williams, 1981). It is well known that the Earth's ring current consists of both electron and ion species. It is found by some event studies that during the main phase of the storm the ions with energies  $E < 50$  keV contribute more significantly to the ring current than those with higher energies. However, during recovery phase and quiet time the contribution of higher energy protons to ring current dominates (Keika et al., 2011; Zhao et al., 2015). The populations of westward drifting ions, and eastward drifting electrons of ring current energy intensify significantly with the increase in geomagnetic activity (Jordanova & Miyoshi, 2005; Le et al., 2004). The spatial and temporal development of the ring current depends strongly on the magnetic field topology in the inner magnetosphere. Ring current causes the global depression in the geomagnetic field observed on the ground during geomagnetic storms. The Dst (disturbance storm time) index has been used as standard measure of ring current strength (Sugiura, 1964). The decrease in Dst index is directly related to the total energy of the ring current particles (Dessler & Parker, 1959; Sckopke, 1966). It is generally understood that the storm time convection intensifies the ring current during the main phase

of the storm (Miyoshi & Kataoka, 2005). Plasma pressure gradients play a very important role in plasma dynamics and the generation of electric currents in the inner magnetosphere. Thus, it is essential to understand the ring current pressure variation and the dynamic changes in the spatial structure of ring current ions and electrons.

Various loss processes can influence the intensity of the ring current. The main mechanism for ring current decay is charge exchange with neutral hydrogen of geocorona (Dessler & Parker, 1959). Ring current particles can also lose energy and be scattered by the plasmaspheric ions and electrons due to Coulomb collisions (Jordanova et al., 1996). Other important mechanism for ring current decay is via pitch angle scattering, due to the resonant interaction of particles with waves, such as Electromagnetic Ion Cyclotron (Cao et al., 2019, 2020; Cornwall et al., 1970; Jordanova et al., 2001; Miyoshi et al., 2008; Summers et al., 2007) and whistler waves (Kozyra et al., 1994). Escape through the dayside magnetopause is also one of the loss processes for ring current particles (Keika et al., 2005, 2006 and references therein). Field line curvature scattering also contributes to the loss of ring current particles and it depends on the geomagnetic activity and location (Delcourt et al., 1996; Tsyganenko, 1982; S. L. Young et al., 2002, 2008; Yu et al., 2020). It is well known that during quiet times, the ion pressure in the inner magnetosphere is dominated by  $H^+$ , while  $O^+$  ion contribution to the ring current pressure increases significantly during storm times and even dominates during very intense storms (Daglis et al., 1999; Greenspan & Hamilton, 2002; Hamilton et al., 1988; Keika et al., 2013; Nosé et al., 2005). Previous studies using in situ observations and modeling have confirmed that during active times,  $O^+$  ions that originate in the ionosphere contribute significantly to the plasma pressure in the inner magnetosphere (Daglis et al., 1999; Ebihara et al., 2006; Fok et al., 2001; Kistler et al., 2016; Yue et al., 2011; Keika et al., 2018). It is also found that warm  $O^+$  dominates close to the plasmopause whereas warm  $H^+$  dominates at higher  $L$ -shells (Jahn et al., 2017).

There are numerous studies on ring current ion composition through observations (Daglis et al., 1999; Greenspan & Hamilton, 2002; Hamilton et al., 1988) and modeling (Jordanova et al., 1996, 2006, 2010). However, the contribution of electrons to the ring current is not well understood. There are few studies which have focused on the role of electrons in the formation of the storm time ring current. An initial study by Frank (1967) showed that electrons contribute to  $\sim 25\%$  to the ring current during active times. Later, Liu et al. (2005) showed that this may be an overestimation because the high energy particles were not included in the study. They showed that during quiet time electrons contribute 1% to the ring current and  $\sim 8\%$ – $19\%$  of the ring current during active time (Liu et al., 2005). The storm time electrons play an important role specially on dawn side and their contribution to ring current is significant (Liu et al., 2005). Jordanova and Miyoshi (2005) extended their global drift loss model to relativistic energies and electrons. They predicted that the electrons contribute to  $\sim 2\%$  during quiet times and their contribution increases to  $\sim 10\%$  during active times. The ring current atmosphere interactions model (RAM) coupled with a self-consistent (SC) magnetic field ( $B$ ) have been successfully used in many ring current studies over decades (Jordanova & Miyoshi, 2005; Jordanova et al., 1996, 2006, 2010, 2016; Yu et al., 2017; Zaharia et al., 2006). Jordanova et al. (2012) showed that the electron contribution to the ring current may reach  $\sim 20\%$  near the peak of a high-speed stream driven storm and should be investigated carefully. Zhao et al. (2016) have also showed that electron has non-negligible contribution to the ring current energy content. They showed contribution of electrons to the ring current  $\sim 12\%$  and  $\sim 7\%$  for a selected moderate and intense storm respectively. They also showed through statistical study that during the main phase of the storms the electron density is higher at midnight and dawn while lower at noon and dusk sector. In this work, we studied the ring current variation during the moderate geomagnetic storm of 7–8 November 2017 using observations and RAM-SCB simulations. We specially focused on electron contribution to the ring current and ground magnetic depression during the magnetic storm that have not been examined previously.

## 2. Data Set and Methodology

Ground magnetic variations (Dst and Sym- $H$  index) are often used as a proxy to understand the evolution of ring current during magnetic storms (Iyemori et al., 1992; Sugiura & Kamei, 1991). However, Dst and Sym- $H$  indices are not sufficient to study the spatial/longitudinal variation in the ring current due to limited number of stations used in their calculation. Therefore, to study these variations more precisely 30 low to midlatitudes ( $09^\circ$ – $45^\circ$ ) ground magnetic stations are used in the present analysis. Table 1 provides the

**Table 1**  
*List of Geomagnetic Observatories Used for the Present Analysis*

Station name	IAGA code	Geographic latitude	Geographic longitude	CGM latitude	CGM longitude
Alibag	ABG	18.64	72.87	12.08	145.46
Apia	API	-13.8	188.22	-15.6	262.65
Alice Springs	ASP	-23.76	133.88	-33.59	207.89
Beijing Ming Tombs	BMT	40.3	116.2	34.99	190.05
Stennis Space Centre	BSL	30.4	270.4	41.2	340.95
Chambon la Foret	CLF	48	2.3	43.33	79.19
Charters Towers	CTA	-20.1	146.3	-29.08	220.48
Fresno	FRN	37.1	240.3	42.98	303.97
Guimar-Tenerife	GUI	28.32	343.56	17.17	60.51
Hartebeesthoek	HBK	-25.88	27.7	-35.74	96.46
Hermanus	HER	-34.4	19.2	-42.33	82.9
Honolulu	HON	21.3	202	21.32	270.06
Jaipur	JAI	26.91	75.8	21.55	149.06
Kakioka	KAK	36.23	140.19	29.31	212.04
Kakadu	KDU	-12.6	132.5	-21.73	204.86
Kanoya	KNY	31.42	130.88	24.87	203.51
Kourou	KOU	5.21	307.27	9.46	23.62
Learmonth	LRM	-22.22	114.1	-32.46	186.53
Lanzhou	LZH	36.08	103.84	30.96	177.23
Memambetsu	MMB	43.9	144.2	37.12	215.74
Phuthuy	PHU	21.03	105.96	14.16	177.96
Pamatai	PPT	-17.6	210.4	-16.72	285.42
San Juan	SJG	18.11	293.85	27.46	10.73
San Pablo-Toledo	SPT	39.5	355.6	31.9	71.78
Tamanrasset	TAM	22.79	5.53	9.22	78.37
Teoloyucan	TEO	19.8	260.8	28.67	331
Trelew	TRW	-43.3	294.7	-29.94	4.92
Tsumeb	TSU	-19.2	17.58	-30.16	88.12
Tucson	TUC	32.2	249.2	39.76	314.86
Vassouras	VSS	-22.4	316.35	-19.63	23.7

details of the 30 stations used in the present analysis. Figure 1 shows the distribution of ground magnetic stations used across the globe. The  $\Delta H$  of each station is calculated using the below equation.

$$\Delta H = \frac{H - H_q}{\cos \varphi} \quad (1)$$

where,  $H$  is a northward component,  $H_q$  is the solar quiet variation averaged over 5 quietest days of that month, and  $\varphi$  is the magnetic latitude of that particular station.

The mean variation  $\Delta H_m$  is calculated using a method described by Li et al. (2011) and Kumar et al., (2020).

$$\Delta H_m = \frac{1}{N} \sum_{n=1}^N \Delta H \quad (2)$$

where  $\Delta H$  is calculated from Equation 1 and  $N$  is the total number of stations.

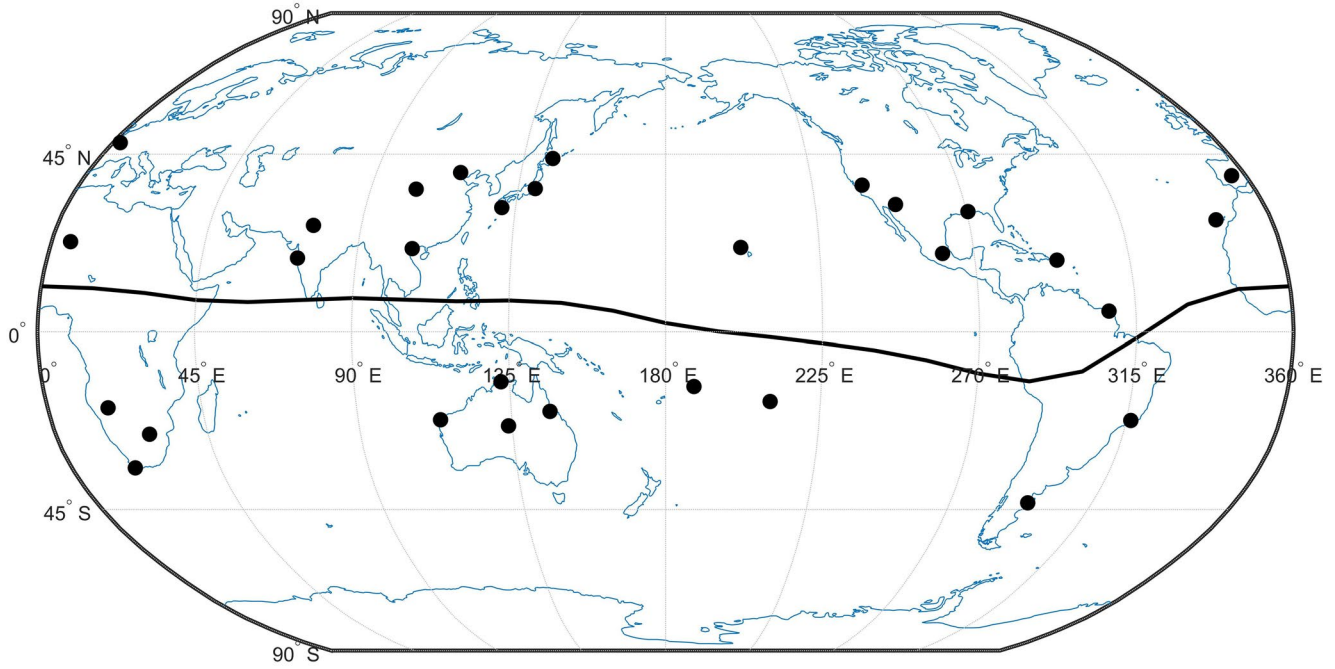


**Figure 1.** Distribution of ground magnetic stations. The black line denotes the magnetic equator.

The Exploration of energization and Radiation in Geospace (ERG) satellite, also known as Arase, has an elliptical orbit with a perigee of 400 km, an apogee of 32,000 km altitude with an inclination of 31° (Miyoshi, Shinohara, et al., 2018). In the present analysis, we use ion data ( $H^+$ ,  $He^+$ , and  $O^+$ ) obtained from low-energy particle experiments-ion mass analyzer (LEP-i [10 eV/q–25 keV/q]) (Asamura et al., 2018b; Asamura, Kasama, et al., 2018), medium-energy particle experiments-ion mass analyzer (MEP-i [10–180 keV/q]) (Yokota et al., 2017, 2018a, 2018b) and the electron data from low-energy particle experiments-electron analyzer (LEP-e [19 eV–20 keV]) (Kazama et al., 2017; Wang et al., 2018a, 2018b), medium-energy particle experiments-electron analyzer (MEP-e [7–87 keV]) (Kasahara et al., 2018a; Kasahara, Yokota, Mitani, et al., 2018) and high-energy particle experiments-electron analyzer (HEP-L [70 keV–2 MeV]) (Mitani et al., 2018a, 2018b) instruments on board Arase satellite.

### 3. RAM-SCB Model

The physics based numerical model used in the present study is the ring current-atmosphere interactions model (RAM) coupled with a SC magnetic field ( $B$ ) (Jordanova & Miyoshi, 2005; Jordanova et al., 1996, 1997, 2006, 2010, 2016; Miyoshi et al., 2006; Yu et al., 2012, 2017; Zaharia et al., 2006). RAM-SCB solves numerically the bounce averaged kinetic equation for the phase distribution function  $Q_l(R_0, \phi, E, \mu_0, t)$  for species  $l$  in the relativistic case using relativistic factor  $\gamma = 1 + \frac{E}{m_0 c^2}$  where  $E$  is the kinetic energy of the particle,  $m_0$  is the rest mass and  $c$  is the speed of light.

$$\begin{aligned} \frac{\partial Q_l}{\partial t} + \frac{1}{R_0^2} \frac{\partial}{\partial R_0} \left( R_0^2 \left\langle \frac{dR_0}{dt} \right\rangle Q_l \right) + \frac{1}{\partial \phi} \left( \left\langle \frac{d\phi}{dt} \right\rangle Q_l \right) + \frac{1}{\gamma p} \frac{\partial}{\partial E} \left( \gamma p \left\langle \frac{dE}{dt} \right\rangle Q_l \right) \\ + \frac{1}{h(\mu_0) \mu_0} \frac{\partial}{\partial \mu_0} \left( h(\mu_0) \mu_0 \left\langle \frac{d\mu_0}{dt} \right\rangle Q_l \right) = \left\langle \left( \frac{\partial Q_l}{\partial t} \right)_{\text{loss}} \right\rangle \end{aligned} \quad (3)$$

Here the brackets  $\langle \rangle$  denotes the bounce averaging,  $p$  is the relativistic momentum of the particle,  $R_0$  is the radial distance in the equatorial plane from  $2 R_E$  to  $6.5 R_E$ ,  $\phi$  is the geomagnetic east longitude, and  $\mu_0$  is

the cosine of the equatorial pitch angle  $\alpha_0$ , where  $\alpha_0$  is from  $0^\circ$  to  $90^\circ$ . The kinetic energy ( $E$ ) of the particle is from 100 eV to 400 keV.  $h$  is proportional to the bounce period along magnetic field lines and defined as

$$h(\mu_0) = \frac{1}{2R_0} \int \frac{ds}{\sqrt{1 - \frac{B(s)}{B_m}}} \quad (4)$$

Here  $B_m$  is the magnetic field at the mirror point,  $ds$  is the distance interval along the field line. The outside boundary conditions are determined from plasma sheet flux measurements from the Magnetospheric Plasma Analyzer and Synchronous Orbit Particle Analyzer instruments on the Los Alamos National Laboratory geosynchronous spacecraft. These measured fluxes are decomposed into different species using the statistical method derived by D. T. Young et al. (1982). The electric field is provided by the latest version of the solar wind-driven W05 (Weimer, 2005) ionospheric model by mapping it along the SCB field lines to the equatorial plane. As for the magnetic field condition, the ring current model is coupled self-consistently to a 3-D force-balanced equilibrium code that computes the magnetic field from the anisotropic RAM plasma conditions (Zaharia et al., 2004, 2006). The loss term in the right-hand side of Equation 3 contains charge exchange loss with geocoronal hydrogen, and loss due to atmospheric precipitation through wave particle interaction.

#### 4. Results

We investigated the ring current variation during the Corotating Interaction Region (CIR) driven moderate storm of 7–8 November 2017. Figure 2 shows the interplanetary parameters in Geocentric Solar Magnetic coordinates and geomagnetic indices during 7–8 November 2017 with 1-min resolution. The variation of solar wind velocity ( $V_{sw}$ ), temperature ( $T$ ), dynamic pressure ( $P$ ), IMF  $B_z$ , auroral index (AL), and Sym- $H$  are shown in Figure 2 from top to bottom (a–f) respectively. An interplanetary shock was observed at  $\sim 0200$  UT on 7 November followed by an increase in solar wind velocity, temperature and solar wind dynamic pressure (Figures 2a–2c). Solar wind velocity started increasing at  $\sim 0200$  UT on 7 November and remained constant ( $\sim 600$  km/s) for the rest of the interval. The solar wind temperature also increased at  $\sim 0200$  UT and was almost constant for the rest of the interval. There were some strong pressure pulses at  $\sim 0300$  UT and  $\sim 0900$  UT. IMF  $B_z$  started fluctuating around 0200 UT. A strong southward excursion to about  $-15$  nT occurred at  $\sim 0800$  UT followed by north-south fluctuations for the rest of the interval. These IMF conditions triggered a moderate geomagnetic storm with minimum Sym- $H = -89$  nT at  $\sim 0400$  UT on 8 November 2017. The main phase of the storm started  $\sim 0800$  UT (shown by vertical line). The minimum AL =  $-1,400$  nT was reached at  $\sim 1300$  UT on 8 November 2017. This is a typical CIR-driven storm, that is, long-lasting recovery phase driven by series of substorms (e.g., Miyoshi & Kataoka, 2008; Miyoshi et al., 2013; Tsurutani et al., 2006).

Figure 3 shows the orbit of Arase satellite in solar magnetic (SM) coordinates (a) in  $X$ - $Y$  plane (b) in  $Z - \sqrt{(X^2 + Y^2)}$  during 7–8 November 2017. The Arase satellite was located in afternoon to dusk sector for most of the time. This location was ideal to observe the ring current particles for the selected storm. To investigate the ring current, we compare the particle fluxes from RAM-SCB simulations driven by solar wind-dependent W05 convection electric field model with observations from the Arase satellite. The flux along the orbit of Arase is obtained using the same MLAT, MLT, and  $L$ -values from RAM simulation.

Figure 4 shows the energy-time diagram of omni-directional ion fluxes of Arase obtained from LEP-i and MEP-i and from RAM-SCB simulations during 7–8 November 2017. Figures 4a and 4b show the  $H^+$  flux from RAM-SCB and Arase observations respectively. The dotted black vertical line represents the onset of main phase. It can be seen that there is increase in  $H^+$  fluxes at all energies after the onset of main phase in both panels RAM-SCB and Arase. There are some data gaps in Figure 4b as the Arase was operating in time of flight mode. The increase in  $H^+$  flux can be seen throughout the main phase. Figures 4c and 4d show the  $O^+$  flux from RAM-SCB and Arase observations respectively. The  $O^+$  fluxes also increased with the onset of main phase in both Arase observations and simulations. Similarly, Figures 4e and 4f shows the  $He^+$  fluxes. There is increase in  $He^+$  fluxes during main phase but not as much compared to  $H^+$  and  $O^+$  fluxes. Figure 4 shows clearly that there was increase in the ions fluxes during main phase indicating the development of

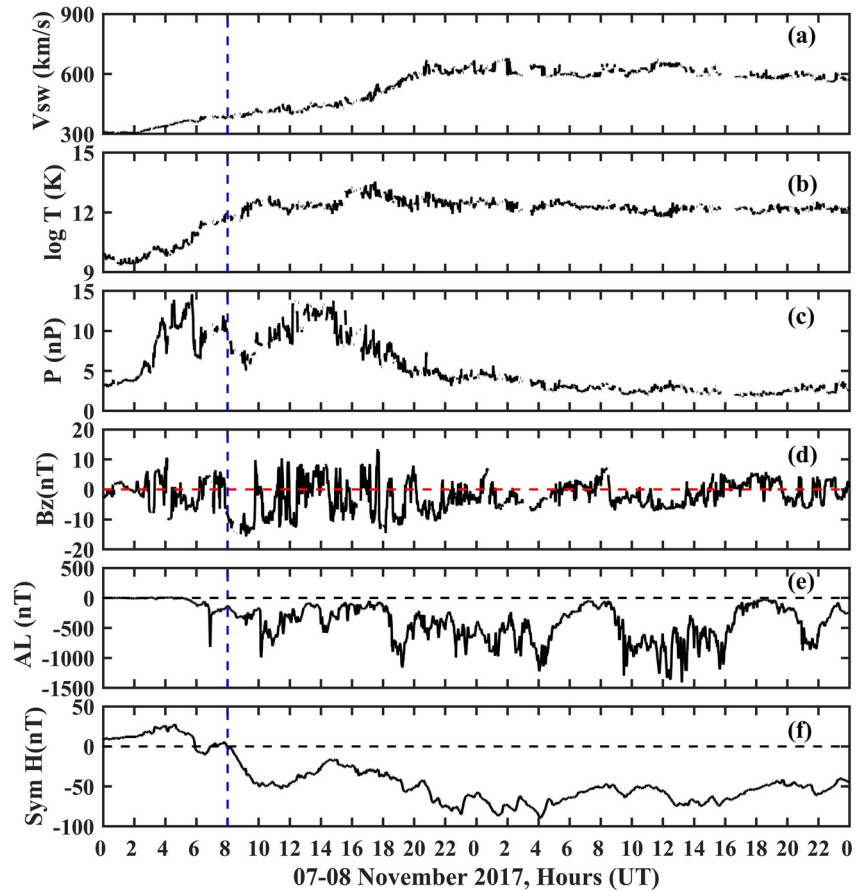


**Figure 2.** Variation in the interplanetary parameters and geomagnetic indices for geomagnetic storm on 7–8 November 2017. Each panel from top to bottom show (a) solar wind velocity ( $V_{sw}$ ), (b) solar wind temperature ( $T$ ), (c) solar wind dynamic pressure ( $P_{sw}$ ), (d) interplanetary magnetic field  $B_z$ , (e) auroral index (AL), and (f) Sym- $H$ . Vertical blue line denotes the onset of main phase of the storm.

ring current. It is also to be noted that RAM-SCB reproduces the observed ion fluxes by Arase satellite very well. Figure 5 shows the energy time diagram of electron fluxes calculated from RAM-SCB and Arase observations obtained from LEP-e, MEP-e, and HEP-L during 7–8 November 2017. It can be seen that there is significant increase in the electron flux after main phase onset in both panels of Figure 5. The electron flux increases initially for few kiloelectron volts (keV) then with the onset of substorms  $\sim 1000$  UT onwards the flux in range of 10 keV to few 100 keV also increased in both panels. However, there are some discrepancies too. The comparison between electron fluxes at  $\sim 0800$ – $1000$  UT is not very good. RAM-SCB shows the significant enhancement of electron fluxes of 0.1–10 keV energies however, these flux enhancements are not observed by Arase satellite. The electron fluxes after 1000 UT observed by Arase are reproduced by RAM-SCB fairly well. In addition, the magnitude of 10–100 keV fluxes measured by Arase are at times a magnitude less than simulated by RAM-SCB. The loss processes can be one of the reasons behind these differences as RAM-SCB used in the present study includes electron loss due to atmospheric precipitation through wave particle interactions using empirical electron lifetime (for further details see Jordanova et al., 2012). These lifetimes might not be representing the actual lifetime well during the specific storm conditions. It can be seen from Figures 4 and 5 that RAM-SCB has reproduced the ion and electron fluxes measured by Arase reasonably well.

Figure 6 shows the plasma pressure observed by Arase and RAM-SCB for LEP-i (100 eV/q–20 keV/q), LEP-e (19 eV–20 keV), MEP-i (10 keV/q–170 keV/q), and MEP-e (7–87 keV) energies. The plasma pressure is calculated for each  $p$  particle species using RAM-SCB from the energy ( $E$ ) and pitch angle ( $\alpha$ ) distributions of differential flux  $J(E, \alpha)$  (De Michelis et al., 1999)

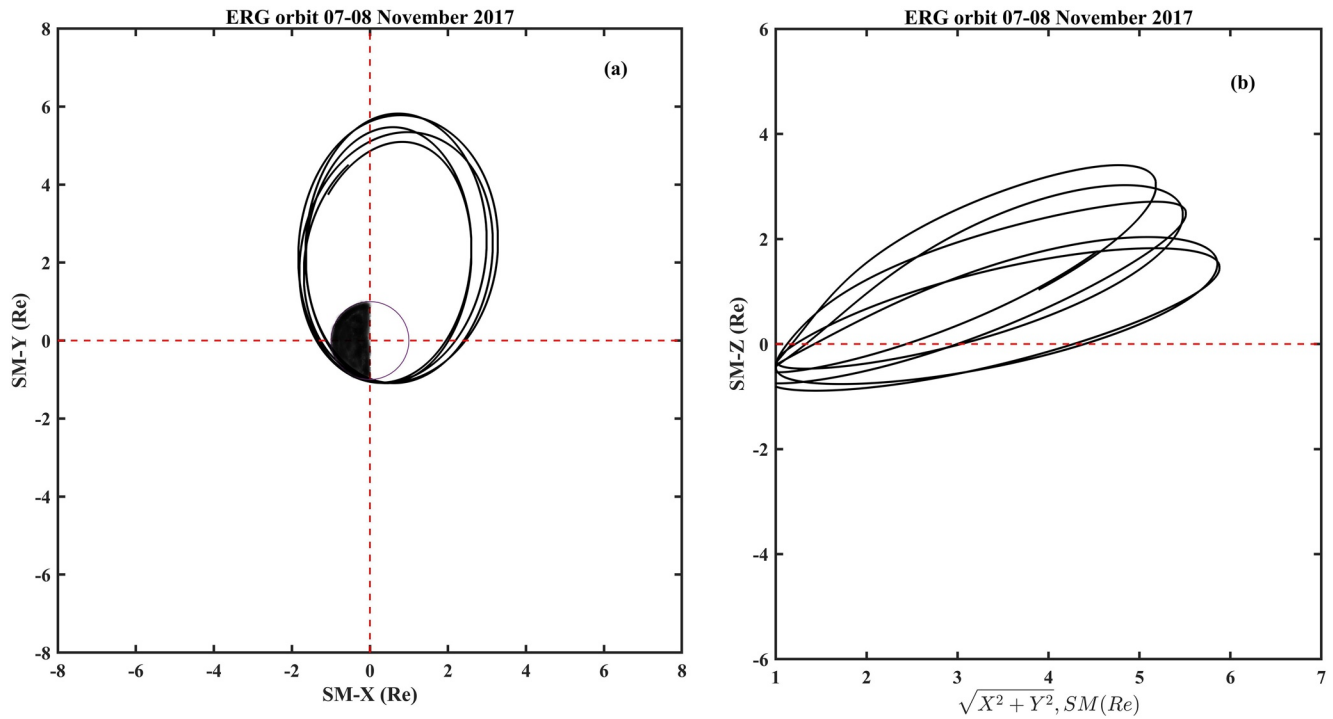


**Figure 3.** Orbit of the Exploration of energization and Radiation in Geospace (ERG) satellite in solar magnetic (SM) coordinates and during 7–8 November 2017 magnetic storm.

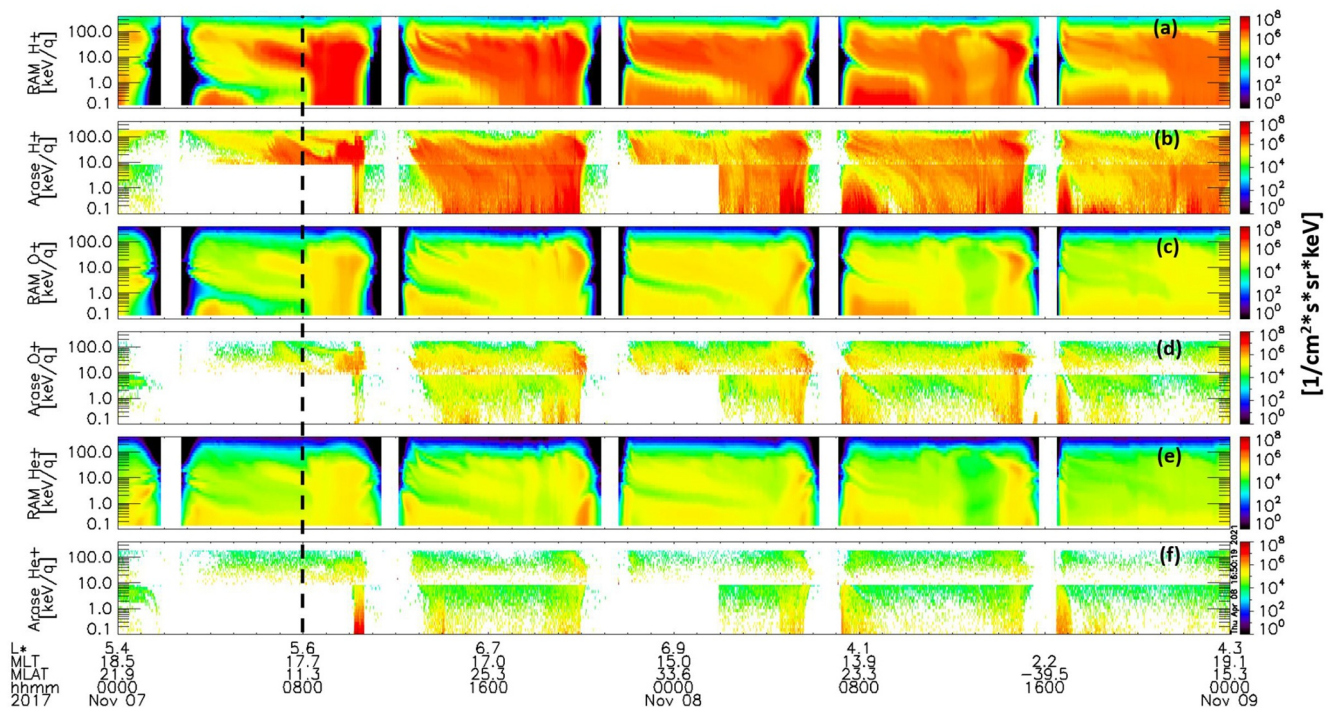


**Figure 4.** Time series of omni-directional ion flux measurements by low-energy particle experiments-ion mass analyzer and medium-energy particle experiments-ion mass analyzer of Arase satellite and Ring current Atmosphere interactions Model with Self Consistent magnetic field (RAM-SCB) calculated fluxes along the Arase orbit. (a) Proton, (c) oxygen, and (e) helium fluxes calculated by RAM-SCB. (b) Proton, (d) oxygen, and (f) helium fluxes measured by Arase satellite. Vertical black line denotes the onset of main phase of the storm.

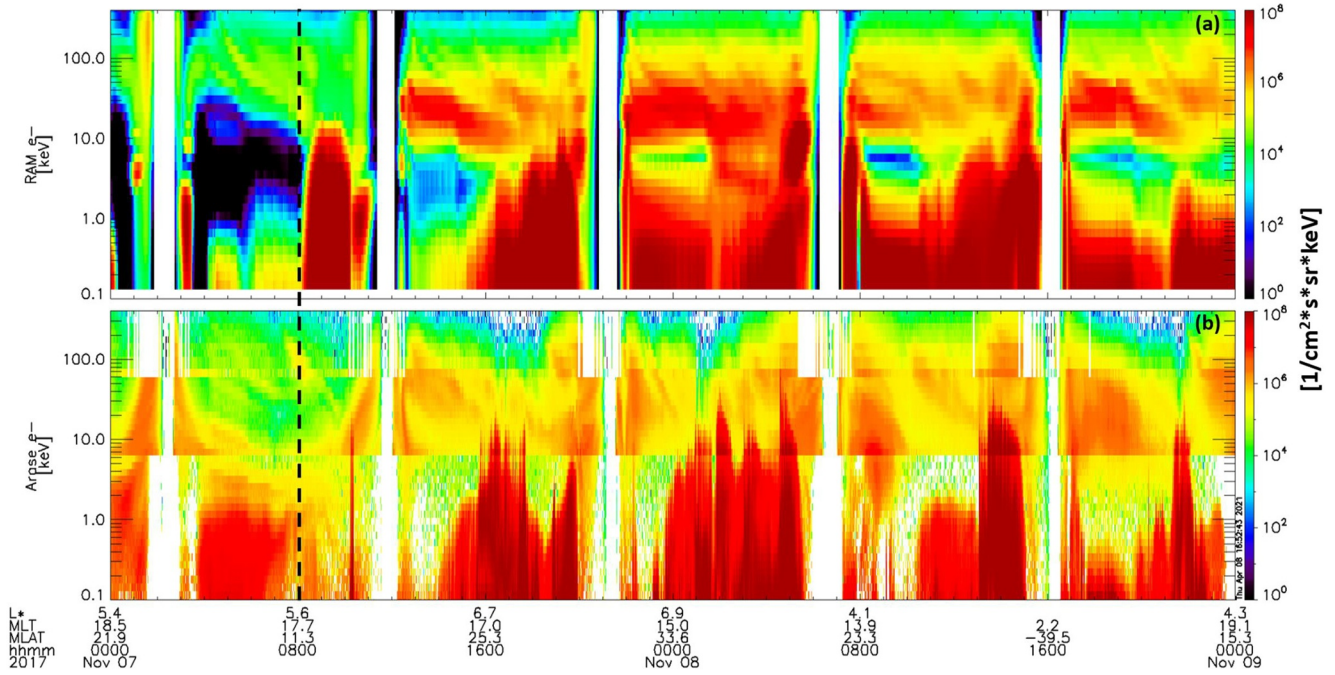


**Figure 5.** Time series of electron flux measurements by Arase satellite and Ring current Atmosphere interactions Model with Self Consistent magnetic field (RAM-SCB) along Arase orbit. (a) Electron omni-directional fluxes calculated by RAM-SCB. (b) Electron omni-directional fluxes measured by Arase satellite. Vertical black line denotes the onset of main phase of the storm.

$$P_{\perp} = \pi \sum_E \sum_{\alpha} \sqrt{2mEJ(E, \alpha)} \sin^3 \alpha \Delta E \Delta \alpha \quad (5)$$

$$P_{\parallel} = 2\pi \sum_E \sum_{\alpha} \sqrt{2mEJ(E, \alpha)} \cos^2 \alpha \sin \alpha \Delta E \Delta \alpha \quad (6)$$

where  $m$  is the mass of the species,  $\Delta E$  is the energy channel width, and  $\Delta \alpha$  is the pitch angle bin width. Figures 6a–6c shows the plasma pressure observed by Arase (red line) and calculated from RAM-SCB (black line) for  $H^+$ ,  $O^+$  (LEP-i) and electrons (LEP-e). It can be seen that ions pressure from Arase and RAM-SCB are very similar except few occasions. The electron pressure (LEP-e) for lower energies RAM-SCB overestimated the observed pressure on November 8 around 0600–0800 UT. Similarly, Figures 6d–6f shows the plasma pressure observed by Arase and RAM-SCB for  $H^+$ ,  $O^+$  (MEP-i), and electrons (MEP-e). The ions pressure is very similar from observation and simulation for MEP-i energies except the 0700 UT on November 8 when RAM-SCB underestimated the proton pressure. It can be seen RAM-SCB reproduced very well the observed plasma pressure by Arase except few occasions especially near boundary cut off of the model. Figure 6f shows the electron pressure from Arase (MEP-e) and RAM-SCB. It can be seen electron pressure also reproduced by RAM-SCB except at 1400 UT on November 8 when model underestimated the plasma pressure.

In order to see the ring current asymmetry, the mean  $\Delta H_m$  (from Equation 2) is subtracted from the  $\Delta H$  of each station to calculate  $\Delta H_{asy}$  ( $\Delta H_{asy} = \Delta H - \Delta H_m$ ) (Kumar et al., 2020). The top panel of Figure 7 shows the variation of  $\Delta H_{asy}$  with 1-min resolution with UT ( $X$ -axis) and MLT ( $Y$ -axis) along with pressure corrected Sym- $H$  (Sym- $H^*$ ) during 7–8 November 2017. The color bar represents the magnitude of  $\Delta H_{asy}$ . Sym- $H^*$  is the value after removing the contribution from the magnetopause currents (Burton et al., 1975; O'Brien & McPherron, 2000) using the following equation:

$$\text{Sym}H^* = \text{Sym}H - b\sqrt{P_d} + c$$



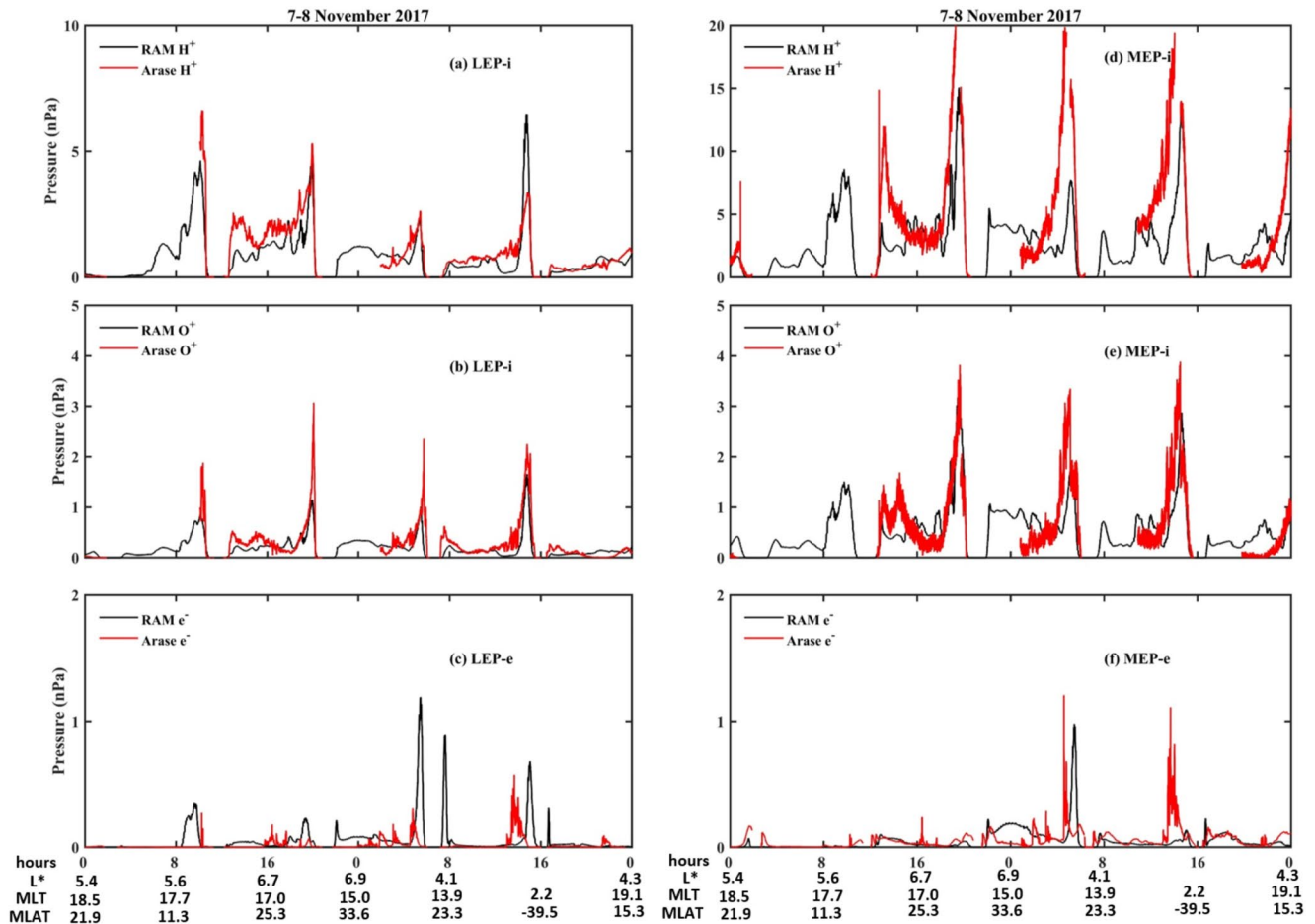


**Figure 6.** Comparison of plasma pressure observed by Arase (red line) and Ring current Atmosphere interactions Model with Self Consistent magnetic field (black line) for low-energy particle experiments-ion mass analyzer (LEP-i) (100 eV/q–20 keV/q) ions (a) H<sup>+</sup>, (b) O<sup>+</sup>, and (c) low-energy particle experiments-electron analyzer (LEP-e) (19 eV–20 keV) electrons. Medium-energy particle experiments-ion mass analyzer (MEP-i) (10 keV/q–170 keV/q) ions (d) H<sup>+</sup>, (e) O<sup>+</sup>, and (f) medium-energy particle experiments-electron analyzer (MEP-e) (7–87 keV) electrons.

where  $b = 7.26$  and  $c = 11$  are the values derived by O'Brien and McPherron (2000) and  $P_d$  is the solar wind dynamic pressure in nPa.

It can be seen from Figure 7 that there is a clear and strong asymmetry in the ring current after 0800 UT (dotted vertical line). It is also to be noted that before 0800 UT, the  $\Delta H_{asy}$  variations show weak asymmetry in the ring current. However, after 0800 UT, dawn sector (0300–0700 MLT) shows the positive  $\Delta H_{asy}$  variations whereas the dusk sector (1700–2100 MLT) shows negative  $\Delta H_{asy}$  variations indicating the ring current is stronger at dusk sector than dawn sector. It is well known that ring current is asymmetric during the main phase of the geomagnetic storm. The ground magnetic depression during geomagnetic storms is caused by the increase in ring current (plasma pressure) in inner magnetosphere. The top panel of Figure 8 shows the variation of the total (integrated over all species) plasma pressure ( $L = 3–6.5$ ) with UT and MLT, and the bottom panel shows the Sym- $H^*$  variations during 7–8 November 2017. It can be seen ~0400 UT there was increase in plasma pressure in dusk sector, which might have caused the initial depression in Sym- $H^*$ . There was significant increase in plasma pressure ~0800 UT (marked with vertical line) at dusk and post-midnight sector. During the same time there was a significant decrease in the Sym- $H^*$ . The plasma pressure also shows similar asymmetric variation as shown by ground magnetic stations in Figure 7. This again shows that the ring current is asymmetric during the main phase of the geomagnetic storm. The ratio of individual species pressure to the total pressure was calculated to investigate their contribution to the total ring current and shown in Figure 9. Figure 9a shows the ratio of H<sup>+</sup> pressure to the total pressure ( $P_T$ ) integrated over  $L = 3–6.5$  during 7–8 November 2017. It can be seen that the H<sup>+</sup> pressure dominates

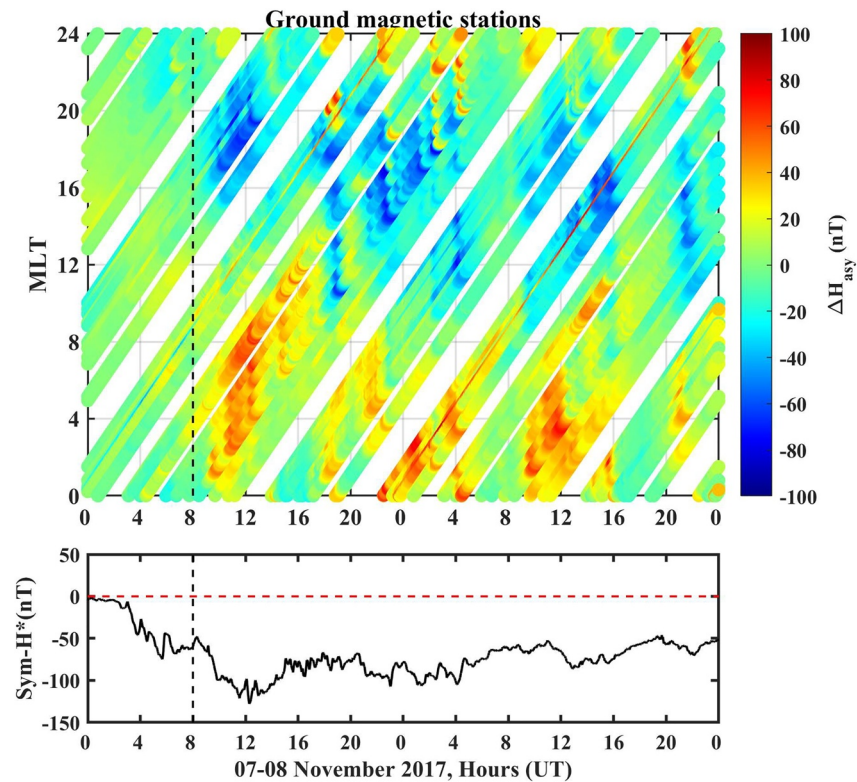


**Figure 7.** (Top panel) variation of  $\Delta H_{asy} = \Delta H - \Delta H_m$  with MLT and onset time (UT). (Bottom panel) variation of pressure corrected Sym- $H^*$  index during the magnetic storm of 7–8 November 2017.

at afternoon to dusk sector after the onset of main phase (vertical dotted line). Figures 9b and 9c show the ratio of  $O^+$  and  $He^+$  to the total pressure respectively. It can be seen from Figures 9a–9c that the ion pressure is dominating in dusk to post-midnight sector. Figure 9d shows the ratio of electrons pressure to the total pressure during 7–8 November 2017. The electron pressure is enhanced in midnight to dawn sector with peak plasma pressure at dawn sector. Note that  $H^+$  has the highest ratio to the total pressure ( $\sim 0.8$ ). It can be seen clearly from Figure 9 that the ion pressure is dominating in dusk sector whereas the electron pressure is dominating in dawn sector.

In order to see the electron contribution to the ring current in the dawn sector, the electron pressure at 0300–0800 MLT has been plotted in Figure 10 along with the ground  $\Delta H$  variations (Equation 1). The top panel in Figure 10a shows the ground  $\Delta H$  variations at 0300–0800 MLT sector during 1600–1200 UT on 7–8 November 2017 while bottom panel shows the variation of Sym- $H^*$ . Figure 10b shows the total electron pressure in 0300–0800 MLT sector during 1600 UT 7 November until 1200 UT 8 November 2017. It can be seen from Figure 10b that the electron pressure started increasing significantly after 1800 UT on 7 November 2017. The electron pressure was highest at  $\sim 2200$  UT. The ground  $\Delta H$  variations started showing more negative variations during the same period (shown by red color). The enhanced electron pressure has contributed significantly to this negative depression in ground  $\Delta H$  variations near the dawn sector.

## 5. Discussions

Knowledge of the ring current particles composition in the inner magnetosphere is essential for the understanding of magnetospheric processes and related instabilities. The global ground geomagnetic field depression during geomagnetic storms is caused by the ring current. It is well known that the ring current is highly asymmetric during main and early recovery phase during geomagnetic storms and dawn-dusk asymmetry is observed (Ebihara & Ejiri, 2000; Fok et al., 1996; Jordanova et al., 2006; Kumar et al., 2020; Liemohn et al., 1999; Sugiura & Chapman, 1960).

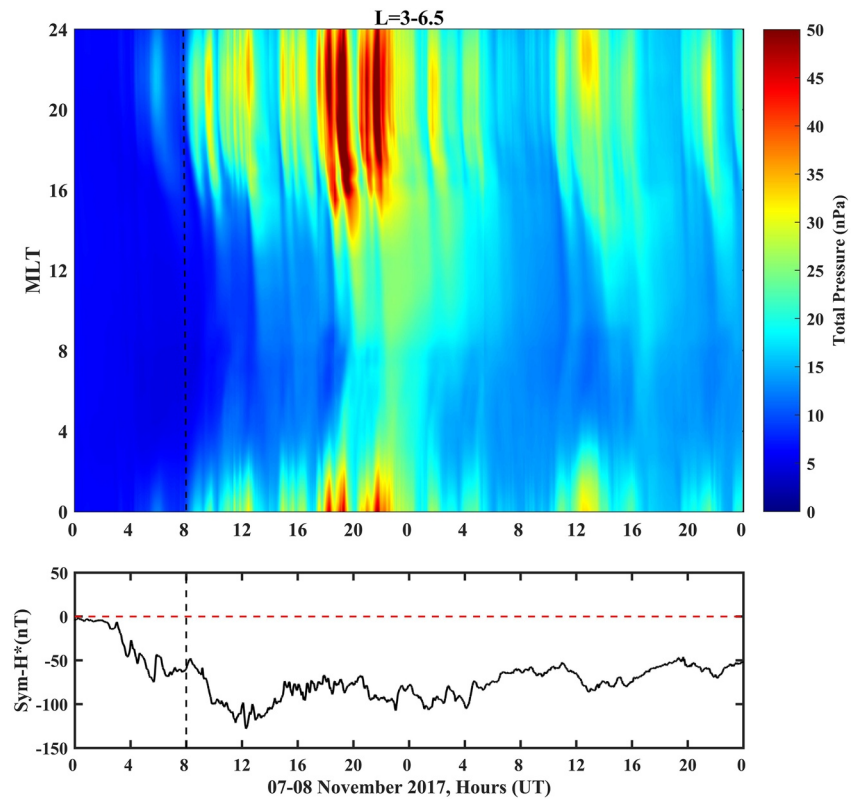


**Figure 8.** (Top) Variation of sum of total pressure (ions + electrons) from  $L = 3-6.5$  with MLT and onset time (UT). (Bottom) Variation of pressure corrected Sym- $H$  (Sym- $H^*$ ) index during the magnetic storm of 7–8 November 2017.

In the present study, we compared the ion and electron fluxes calculated with RAM-SCB with Arase observations. It is found that RAM-SCB simulations reproduce reasonably well the particle fluxes observed by Arase satellite in the inner magnetosphere during 7–8 November 2017 geomagnetic storm. The ion and electron fluxes started to increase during the main phase of the geomagnetic storm. The ion fluxes with energy in 10 keV to few 100 keV increased significantly during the main phase. Similarly, electron fluxes with energy few keV increased initially and with the enhanced substorm activity fluxes with energy 10 keV enhanced significantly. We also compared the plasma pressure observed by Arase and RAM-SCB for LEP-i (100 eV/q–20 keV/q), LEP-e (19 eV–20 keV), MEP-i (10 keV/q–170 keV/q), and MEP-e (7–87 keV) energies. It is found that RAM-SCB reproduces the observed plasma pressure by Arase reasonably well.

Low and middle latitudes ground magnetic variations are often used as a proxy to understand the evolution of ring current during geomagnetic storms. In the present study, we used data from ground magnetic stations to study the ring current variations observed at ground. Storm time ground H component has contribution from various current systems (e.g., magnetopause current, symmetric/asymmetric ring current, tail current and ionospheric currents). However, these currents have different origin and effects at different magnetic local times (Tsyganenko & Sitnov, 2005; Turner et al., 2000; Yu et al., 2010). It is also to be noted that field aligned currents (FACs) also contribute to the ground magnetic field during disturbed time (Imajo et al., 2020). FACs are large scale current system that flows in and out of the ionosphere. Region 2 (R2) FACs flows out and in to the ionosphere on the dawn and dusk side respectively (Iijima & Potemra, 1976). During disturbed time R2 FACs move equatorward and get connected to the ring current in the inner magnetosphere (Liemohn et al., 2016). This closure part of the ring current is known as the partial ring current (PRC) and is formed by the nightside pressure enhancement observed during the main phase of the magnetic storm (Ebihara et al., 2002). Therefore, ring current is asymmetric due to the generation of PRC and a dawn-dusk asymmetry is observed in the ground H-component during the main phase of the magnetic storm. Figure 6 shows a clear dawn-dusk asymmetry of ring current observed at ground magnetic stations. The four-dimensional physics-based model RAM-SCB with self-consistent magnetic field has been

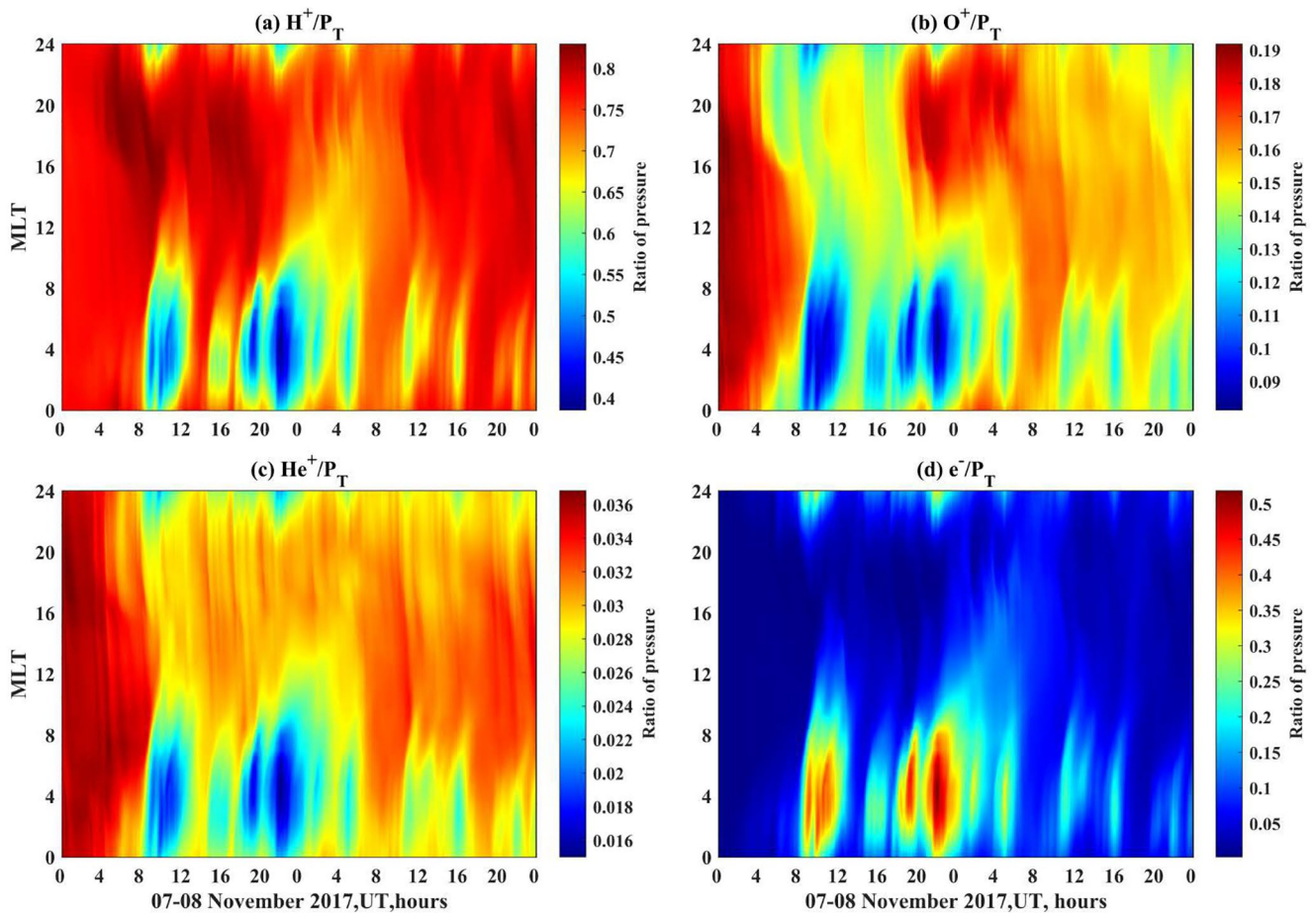


**Figure 9.** Ratio of particle pressure to the total ring current pressure ( $P_T$ ) as a function of MLT and UT (a) proton, (b) oxygen, (c) helium, and (d) electron.

used successfully over the past decade to reproduce ring current dynamics and morphology during various geomagnetic conditions (Jordanova et al., 2006, 2010, 2014, 2016; Yu et al., 2017; Zaharia et al., 2006).

In the present study, we used RAM-SCB simulations to calculate the ring current pressure in the inner magnetosphere during 7–8 November 2017 geomagnetic storm. The ring current intensifies during the main phase of the storm (Figure 7). The ring current pressure is asymmetric as the ring current is stronger in dusk to midnight sector (Figure 7). It is found that the ring current is mainly dominated by the ions. We calculated the contribution of each species to the total ring current pressure. The  $H^+$  and  $O^+$  contribution to ring current was found to be  $\sim 71\%$  and  $\sim 15\%$  respectively during the main phase of the storm.  $He^+$  contribution was found to be  $\sim 2\%$  to the ring current. Interestingly, the electron component contributed  $\sim 12\%$  to the total ring current. However, in the dawn sector the electron contribution to the ring current is important and could increase locally to  $\sim 18\%$  due to substorm injections during the peak of the storm.

## 6. Summary and Conclusions

In the present paper, we investigated the ring current variations during the 7–8 November 2017 magnetic storm using in situ and ground-based observations and RAM-SCB simulations. The ion and electron fluxes in the inner magnetosphere measured by Arase satellite were fairly well reproduced by RAM-SCB simulations. RAM-SCB reproduces the plasma pressure observed by Arase satellite during the storm. The ground magnetic stations show the clear dawn-dusk asymmetry of the ring current. Pressure variations from RAM-SCB show that the ion and electron pressure was dominating in the dusk and dawn sector respectively. During the main phase of the storm the ions contributed  $\sim 88\%$  whereas electrons contributed  $\sim 12\%$  to the total ring current. The ring current was mainly dominated by  $H^+$  ( $\sim 71\%$ ),  $O^+$  contributed  $\sim 15\%$

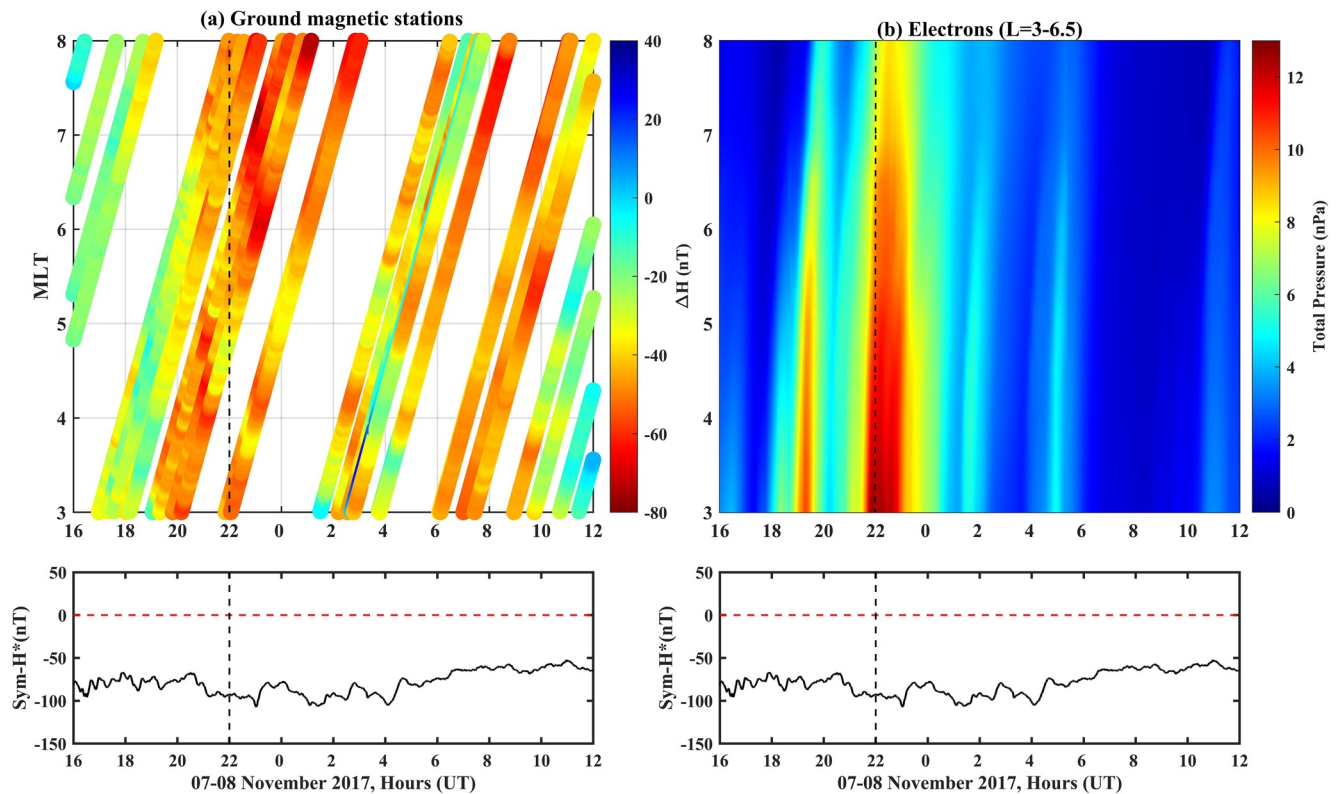


**Figure 10.** (a) Top panel: variation of ground  $\Delta H$  component from 03 to 08 MLT and onset time (UT). Bottom panel: Variation of Sym- $H^*$  index from 1600 to 1200 UT of 7–8 November 2017. (b) Top panel: variation of total electron pressure ( $L = 3-6.5$ ) from 03 to 08 MLT and UT. Bottom panel: variation of Sym- $H^*$  index for 7–8 November 2017. The vertical dash line shows the peak of electron pressure.

and  $\text{He}^+$  contribution was  $\sim 2\%$  during the main phase. Interestingly, it is found that the  $\Delta H$  variation at ground in dawn sector (0300–0800 MLT) sector was negative corresponding to enhanced electron pressure. The majority of ring current pressure is dominated by ions in the dusk sector during the main phase. However, electrons have non-negligible contribution to the ring current in the dawn sector. It is expected that enhanced electron pressure might have contributed to negative  $\Delta H$  variations at ground in the dawn sector. Thus, storm time ring current electrons should be included to estimate the total pressure in future observational and model studies.

### Data Availability Statement

The RAM-SCB model data used in the present study are available at <https://nuss.nagoya-u.ac.jp/s/inLS9sDARSyCJjw>.

### Acknowledgments

Science data of the ERG (Arase) satellite were obtained from the ERG Science Center operated by ISAS/JAXA and ISEE/Nagoya University (<https://ergsc.isee.nagoya-u.ac.jp/index.shtml.en>, Miyoshi, Hori, et al., 2018). The present study analyzed level 2 LEP-i v03\_00 (Asamura et al., 2018a, 2018b) LEP-e L2 v02\_02 (Wang et al., 2018a, 2018b) HEP-L2 v03\_01 (Mitani, Hori, et al., 2018), MEP-e-L2 v01\_02 (Kasahara et al., 2018a, 2018b), MEP-i L2

### References

- Asamura, K., Kazama, Y., Yokota, S., Kasahara, S., & Miyoshi, Y. (2018). Low-energy particle experiments-ion mass analyzer (LEPi) on-board the ERG (Arase) satellite. *Earth, Planets and Space*, 70, 70. <https://doi.org/10.1186/s40623-018-0846-0>
- Asamura, K., Miyoshi, Y., & Shinohara, I. (2018a). *The LEPi instrument Level-2 3-D flux data of Exploration of energization and Radiation in Geospace (ERG) Arase satellite, Version v03\_00*. ERG Science Center, Institute for Space-Earth Environmental Research, Nagoya University. <https://doi.org/10.34515/DATA.ERG-05001>
- Asamura, K., Miyoshi, Y., & Shinohara, I. (2018b). *The LEPi instrument Level-2 omniflux data of Exploration of energization and Radiation in Geospace (ERG) Arase satellite, Version v03\_00*. ERG Science Center, Institute for Space-Earth Environmental Research, Nagoya University. <https://doi.org/10.34515/DATA.ERG-05000>
- Burton, R. K., McPherron, R. L., & Russell, C. T. (1975). An empirical relationship between interplanetary conditions and Dst. *Journal of Geophysical Research*, 80(31), 4204–4214. <https://doi.org/10.1029/JA080i031p04204>
- Cao, X., Ni, B., Summers, D., Shprits, Y. Y., Gu, X., Fu, S., et al. (2019). Sensitivity of EMIC wave-driven scattering loss of ring current protons to wave normal angle distribution. *Geophysical Research Letters*, 46, 590–598. <https://doi.org/10.1029/2018GL081550>

v02\_00 (Yokota et al., 2018a, 2018b), and orbit L2 v02 (Miyoshi, Shinohara, & Jun, 2018) data. The authors thank the Coordinated Data Analysis Web (CDAWeb) (<https://cdaweb.sci.gsfc.nasa.gov/index.html/>) for providing 1-min resolution solar wind interplanetary data. The authors also thank Kyoto World Data Center for Geomagnetism (<http://wdc.kugi.kyoto-u.ac.jp/wdc/Sec3.html>) for providing quiet days of the month, Auroral indices, and Sym-H data. The results presented in this paper rely on data collected at magnetic observatories. The authors thank the national institutes that support them and INTERMAGNET for promoting high standards of magnetic observatory practice ([www.intermagnet.org](http://www.intermagnet.org)). S. Kumar and Y. Miyoshi works are supported by PWING project. The PWING project is funded as the Grant-in-Aid for Specially Promoted Research (16H06286) by the Japan Society for the Promotion of Science and the Ministry of Education, Culture, Sports, Science and Technology. Y. Miyoshi is also supported by Grant-in-Aid for research (15H05815, 15H05747, 20H01959). Work at Los Alamos was conducted under the auspices of the US Department of Energy with partial support from NASA grants 80HQTR19T0023 and 80HQTR19T0058.

- Cao, X., Ni, B., Summers, D., Shprits, Y. Y., & Lou, Y. (2020). Effects of polarization reversal on the pitch angle scattering of radiation belt electrons and ring current protons by EMIC waves. *Geophysical Research Letters*, 47, e2020GL089718. <https://doi.org/10.1029/2020GL089718>
- Cornwall, J. M., Coroniti, F. V., & Thorne, R. M. (1970). Turbulent loss of ring current protons. *Journal of Geophysical Research*, 75(25), 4699–4709. <https://doi.org/10.1029/JA075i025p04699>
- Daglis, I. A., Sarris, E. T., & Wilken, B. (1993). AMPTE/CCE CHEM observations of the energetic ion population at geosynchronous altitudes. *Annales Geophysicae*, 11, 685–696.
- Daglis, I. A., Thorne, R. M., Baumjohann, W., & Orsini, S. (1999). The terrestrial ring current: Origin, formation, and decay. *Reviews of Geophysics*, 37(4), 407–438. <https://doi.org/10.1029/1999RG900009>
- Delcourt, D. C., Sauvaud, J. A., Martin, R. F., Jr., & Moore, T. E. (1996). On the nonadiabatic precipitation of ions from the near-earth plasma sheet. *Journal of Geophysical Research*, 101(A8), 17409–17418. <https://doi.org/10.1029/96JA01006>
- De Michelis, P., Daglis, I. A., & Consolini, G. (1999). An average image of proton plasma pressure and of current systems in the equatorial plane derived from AMPTE/CCE-CHEM measurements. *Journal of Geophysical Research*, 104(A12), 28615–28624. <https://doi.org/10.1029/1999JA900310>
- Dessler, A. J., & Parker, E. N. (1959). Hydromagnetic theory of magnetic storms. *Journal of Geophysical Research*, 64, 2239–2252. <https://doi.org/10.1029/JZ064i012p02239>
- Dungey, J. W. (1961). Interplanetary magnetic field and the auroral zones. *Physical Review Letters*, 6(2), 47–48. <https://doi.org/10.1103/PhysRevLett.6.47>
- Ebihara, Y., & Ejiri, M. (2000). Simulation study on fundamental properties of the storm-time ring current. *Journal of Geophysical Research*, 105(A7), 15843–15859. <https://doi.org/10.1029/1999JA900493>
- Ebihara, Y., Ejiri, M., Nilsson, H., Sandahl, I., Milillo, A., Grande, M., et al. (2002). Statistical distribution of the storm-time proton ring current: POLAR measurements. *Geophysical Research Letters*, 29(20), 1969. <https://doi.org/10.1029/2002GL015430>
- Ebihara, Y., & Miyoshi, Y. (2011). Dynamic inner magnetosphere: A tutorial and recent advance. In W. Liu, & M. Fujimoto (Eds.), *The dynamic magnetosphere* (pp. 145–187). Springer. [https://doi.org/10.1007/978-94-007-0501-2\\_9](https://doi.org/10.1007/978-94-007-0501-2_9)
- Ebihara, Y., Yamada, M., Watanabe, S., & Ejiri, M. (2006). Fate of outflowing suprathermal oxygen ions that originate in the polar ionosphere. *Journal of Geophysical Research*, 111, A04219. <https://doi.org/10.1029/2005JA011403>
- Fok, M.-C., Moore, T. E., & Greenspan, M. E. (1996). Ring current development during storm main phase. *Journal of Geophysical Research*, 101(A7), 15311–15322. <https://doi.org/10.1029/96JA01274>
- Fok, M.-C., Wolf, R. A., Spiro, R. W., & Moore, T. E. (2001). Comprehensive computational model of Earth's ring current. *Journal of Geophysical Research*, 106(A5), 8417–8424. <https://doi.org/10.1029/2000JA000235>
- Frank, L. A. (1967). On the extraterrestrial ring current during geomagnetic storms. *Journal of Geophysical Research*, 72(15), 3753–3767. <https://doi.org/10.1029/JZ072i015p03753>
- Gonzalez, W. D., Joselyn, J. A., Kamide, Y., Kroehl, H. W., Rostoker, G., Tsurutani, B. T., & Vasyliunas, V. (1994). What is a geomagnetic storm. *Journal of Geophysical Research*, 99, 5771–5792. <https://doi.org/10.1029/93JA02867>
- Greenspan, M. E., & Hamilton, D. C. (2002). Relative contributions of H<sup>+</sup> and O<sup>+</sup> to the ring current energy near magnetic storm maximum. *Journal of Geophysical Research*, 107(A4), 1043. <https://doi.org/10.1029/2001JA000155>
- Hamilton, D. C., Gloeckler, G., Ipavich, F. M., Wilken, B., Stuedemann, W., & Kremser, G. (1988). Ring current development during the great geomagnetic storm of February 1986. *Journal of Geophysical Research*, 93(A12), 14343–14355. <https://doi.org/10.1029/JA093iA12p14343>
- Iijima, T., & Potemra, T. A. (1976). The amplitude distribution of field aligned currents at northern high latitudes observed by Triad. *Journal of Geophysical Research*, 81(13), 2165–2174. <https://doi.org/10.1029/JA081i013p02165>
- Imajo, S., Nosé, M., Aida, M., Higashio, N., Matsumoto, H., Kiyokazu, K., et al. (2020). Evolution of field-aligned current in the meridional plane during substorm: Multipoint observations from satellites and ground stations. *Earth, Planets and Space*, 72, 1–9. <https://doi.org/10.1186/s40623-020-01182-6>
- Iyemori, T., Araki, T., Kamei, T., & Takeda, M. (1992). *Mid-latitude geomagnetic indices ASY and SYM (Provisional) No. 1 1989*. Data Analysis Center for Geomagnetism and Space Magnetism, Kyoto University
- Jahn, J. M., Goldstein, J., Reeves, G. D., Fernandes, P. A., Skoug, R. M., Larsen, B. A., & Spence, H. E. (2017). The warm plasma composition in the inner magnetosphere during 2012–2015. *Journal of Geophysical Research: Space Physics*, 122, 11018–11043. <https://doi.org/10.1002/2017ja024183>
- Jordanova, V. K., Farrugia, C. J., Thorne, R. M., Khazanov, G. V., Reeves, G. D., & Thomsen, M. F. (2001). Modeling ring current proton precipitation by electromagnetic ion cyclotron waves during the May 14–16, 1997, storm. *Journal of Geophysical Research*, 106(A1), 7–22. <https://doi.org/10.1029/2000JA002008>
- Jordanova, V. K., Ilie, R., & Chen, M. W. (2020). Introduction and historical background. In *Ring current investigations: The quest for space weather prediction* (pp. 1–13). Elsevier Inc. <https://doi.org/10.1016/B978-0-12-815571-4.00001-9>
- Jordanova, V. K., Kistler, L. M., Kozyra, J. U., Khazanov, G. V., & Nagy, A. F. (1996). Collisional losses of ring current ions. *Journal of Geophysical Research*, 101(A1), 111–126. <https://doi.org/10.1029/95JA02000>
- Jordanova, V. K., Kozyra, J. U., Nagy, A. F., & Khazanov, G. V. (1997). Kinetic model of the ring current-atmosphere interactions. *Journal of Geophysical Research*, 102, 14279–14292. <https://doi.org/10.1029/96JA03699>
- Jordanova, V. K., & Miyoshi, Y. S. (2005). Relativistic model of ring current and radiation belt ions and electrons: Initial results. *Geophysical Research Letters*, 32, L14104. <https://doi.org/10.1029/2005GL023020>
- Jordanova, V. K., Miyoshi, Y. S., Zaharia, S., Thomsen, M. F., Reeves, G. D., Evans, D. S., et al. (2006). Kinetic simulations of ring current evolution during the Geospace Environment Modeling challenge events. *Journal of Geophysical Research*, 111, A11S10. <https://doi.org/10.1029/2006JA011644>
- Jordanova, V. K., Tu, W., Chen, Y., Morley, S. K., Panaitescu, A. -D., Reeves, G. D., & Kletzing, C. A. (2016). RAM-SCB simulations of electron transport and plasma wave scattering during the October 2012 “double-dip” storm. *Journal of Geophysical Research: Space Physics*, 121, 8712–8727. <https://doi.org/10.1002/2016JA022470>
- Jordanova, V. K., Welling, D. T., Zaharia, S. G., Chen, L., & Thorne, R. M. (2012). Modeling ring current ion and electron dynamics and plasma instabilities during a high-speed stream driven storm. *Journal of Geophysical Research*, 117, A00L08. <https://doi.org/10.1029/2011JA017433>
- Jordanova, V. K., Yu, Y., Niehof, J. T., Skoug, R. M., Reeves, G. D., Kletzing, C. A., et al. (2014). Simulations of inner magnetosphere dynamics with an expanded RAM-SCB model and comparisons with Van Allen Probes observations. *Geophysical Research Letters*, 41, 2687–2694. <https://doi.org/10.1002/2014GL059533>

- Jordanova, V. K., Zaharia, S., & Welling, D. T. (2010). Comparative study of ring current development using empirical, dipolar, and self-consistent magnetic field simulations. *Journal of Geophysical Research*, *115*, A00J11. <https://doi.org/10.1029/2010JA015671>
- Kasahara, S., Yokota, S., Hori, T., Keika, K., Miyoshi, Y., & Shinohara, I. (2018). *The MEP-e instrument Level-2 3-D flux data of Exploration of energization and Radiation in Geospace (ERG) Arase satellite, Version v01\_02*. ERG Science Center, Institute for Space-Earth Environmental Research, Nagoya University. <https://doi.org/10.34515/DATA.ERG-02000>
- Kasahara, S., Yokota, S., Hori, T., Keika, K., Miyoshi, Y., & Shinohara, I. (2018). *The MEP-e instrument Level-2 omni-directional flux data of Exploration of energization and Radiation in Geospace (ERG) Arase satellite, Version v01\_02*. ERG Science Center, Institute for Space-Earth Environmental Research, Nagoya University. <https://doi.org/10.34515/DATA.ERG-02001>
- Kasahara, S., Yokota, S., Mitani, T., Asamura, K., Hirahara, M., Shibano, Y., & Takshima, T. (2018). Medium-energy particle experiments-electron analyzer (MEP-e) for the exploration of energization and radiation in geospace (ERG) mission. *Earth, Planets and Space*, *70*, 69. <https://doi.org/10.1186/s40623-018-0847-z>
- Kazama, Y., Wang, B. J., Wang, S. Y., Ho, P. T. P., Tam, S. W. Y., Chang, T. F., et al. (2017). Low-energy particle experiments-electron analyzer (LEPe) onboard the Arase spacecraft. *Earth, Planets and Space*, *69*, 165. <https://doi.org/10.1186/s40623-017-0748-6>
- Keika, K., Brandt, P. C., Nosé, M., & Mitchell, D. G. (2011). Evolution of ring current ion energy spectra during the storm recovery phase: Implication for dominant ion loss processes. *Journal of Geophysical Research*, *116*, A00J20. <https://doi.org/10.1029/2010JA015628>
- Keika, K., Kasahara, S., Yokota, S., Hoshino, M., Seki, K., Nosé, M., et al. (2018). Ion energies dominating energy density in the inner magnetosphere: Spatial distributions and composition, observed by Arase/MEP-i. *Geophysical Research Letters*, *45*, 12153–12162. <https://doi.org/10.1029/2018GL080047>
- Keika, K., Kistler, L. M., & Brandt, P. C. (2013). Energization of O<sup>+</sup> ions in the Earth's inner magnetosphere and the effects on ring current buildup: A review of previous observations and possible mechanisms. *Journal of Geophysical Research: Space Physics*, *118*, 4441–4464. <https://doi.org/10.1002/jgra.50371>
- Keika, K., Nose, M., Brandt, P., Ohtani, S., Mitchell, D. G., & Roelof, E. C. (2006). Contribution of charge exchange loss to the storm time ring current decay: IMAGE/HENA observations. *Journal of Geophysical Research*, *111*, A11S12. <https://doi.org/10.1029/2006JA011789>
- Keika, K., Nose, M., Ohtani, S.-I., Takahashi, K., Christon, S. P., & McEntire, R. W. (2005). Outflow of energetic ions from the magnetosphere and its contribution to the decay of the storm time ring current. *Journal of Geophysical Research*, *110*, A09210. <https://doi.org/10.1029/2004JA010970>
- Kistler, L. M., Mouikis, C. G., Spence, H. E., Menz, A. M., Skouf, R. M., Funsten, H. O., et al. (2016). The source of O<sup>+</sup> in the storm time ring current. *Journal of Geophysical Research: Space Physics*, *121*, 5333–5349. <https://doi.org/10.1002/2015JA022204>
- Kozyra, J. U., Rasmussen, C. E., Miller, R. H., & Lyons, L. R. (1994). Interaction of ring current and radiation belt protons with ducted plasmaspheric hiss: 1. Diffusion coefficients and timescales. *Journal of Geophysical Research*, *99*(A3), 4069–4084. <https://doi.org/10.1029/93JA01532>
- Kumar, S., Veenadhari, B., Chakrabarty, D., Tulasi Ram, S., Kikuchi, T., & Miyoshi, Y. (2020). Effects of IMF By on ring current asymmetry under southward IMF Bz conditions observed at ground magnetic stations: Case studies. *Journal of Geophysical Research: Space Physics*, *125*, e2019JA027493. <https://doi.org/10.1029/2019JA027493>
- Le, G., Russell, C. T., & Takahashi, K. (2004). Morphology of the ring current derived from magnetic field observations. *Annales Geophysicae*, *22*, 1267–1295. <https://doi.org/10.5194/angeo-22-1267-2004>
- Li, H., Wang, C., & Kan, J. R. (2011). Contribution of the partial ring current to the SYMH index during magnetic storms. *Journal of Geophysical Research*, *116*, A11222. <https://doi.org/10.1029/2011JA016886>
- Liemohn, M. W., Ganushkina, N. Y., Ilie, R., & Welling, D. T. (2016). Challenges associated with near-Earth nightside current. *Journal of Geophysical Research: Space Physics*, *121*, 6763–6768. <https://doi.org/10.1002/2016JA022948>
- Liemohn, M. W., Kozyra, J. U., Jordanova, V. K., Khazanov, G. V., Thomsen, M. F., & Cayton, T. E. (1999). Analysis of early phase ring current recovery mechanisms during geomagnetic storms. *Geophysical Research Letters*, *26*(18), 2845–2848. <https://doi.org/10.1029/1999GL900611>
- Liu, S., Chen, M. W., Roeder, J. L., Lyons, L. R., & Schulz, M. (2005). Relative contribution of electrons to the storm time total ring current energy content. *Geophysical Research Letters*, *32*, L03110. <https://doi.org/10.1029/2004GL021672>
- Mitani, T., Hori, T., Park, I., Takashima, T., Miyoshi, Y., & Shinohara, I. (2018). *The HEP instrument Level-2 omni-directional flux data of Exploration of energization and Radiation in Geospace (ERG) Arase satellite*. <https://doi.org/10.34515/DATA.ERG-01001>
- Mitani, T., Takashima, T., Kasahara, S., Miyake, W., & Hirahara, M. (2018). High-energy electron experiments (HEP) aboard the ERG (Arase) satellite. *Earth, Planets and Space*, *70*, 77. <https://doi.org/10.1186/s40623-018-0853-1>
- Miyoshi, Y., Shinohara, I., & Jun, C.-W. (2018). *The level-2 orbit data of exploration of energization and radiation in Geospace (ERG) Arase satellite, version v03*. ERG Science Center, Institute for Space-Earth Environmental Research, Nagoya University. <https://doi.org/10.34515/DATA.ERG-12000>
- Miyoshi, Y. S., Hori, T., Shoji, M., Teramoto, M., Chang, T. F., Segawa, T., et al. (2018). The ERG science center. *Earth, Planets and Space*, *70*(1), 1–11. <https://doi.org/10.1186/s40623-018-0867-8>
- Miyoshi, Y. S., Jordanova, V. K., Morioka, A., Thomsen, M. F., Reeves, G. D., Evans, D. S., & Green, J. C. (2006). Observations and modeling of energetic electron dynamics during the Oct. 2001 storm. *Journal of Geophysical Research*, *111*, A11S02. <https://doi.org/10.1029/2005JA011351>
- Miyoshi, Y. S., & Kataoka, R. (2005). Ring current ions and radiation belt electrons during geomagnetic storms driven by coronal mass ejections and corotating interaction regions. *Geophysical Research Letters*, *32*, L21105. <https://doi.org/10.1029/2005GL024590>
- Miyoshi, Y. S., & Kataoka, R. (2008). Flux enhancement of the outer radiation belt electrons after the arrival of stream interaction regions. *Journal of Geophysical Research*, *113*, A03S09. <https://doi.org/10.1029/2007JA012506>
- Miyoshi, Y. S., Kataoka, R., Kasahara, Y., Kumamoto, A., Nagai, T., & Thomsen, M. (2013). High-speed solar wind with southward interplanetary magnetic field causes relativistic electron flux enhancement of the outer radiation belt via enhanced condition of whistler waves. *Geophysical Research Letters*, *40*, 4520–4525. <https://doi.org/10.1002/grl.50916>
- Miyoshi, Y. S., Sakaguchi, K., Shiokawa, K., Evans, D., Albert, J., Connors, M., & Jordanova, V. (2008). Precipitation of radiation belt electrons by EMIC waves, observed from ground and space. *Geophysical Research Letters*, *35*, L23101. <https://doi.org/10.1029/2008GL035727>
- Miyoshi, Y. S., Shinohara, I., Takashima, T., Asamura, K., Higashio, N., Mitani, T., et al. (2018). Geospace exploration project ERG. *Earth, Planets and Space*, *70*, 101. <https://doi.org/10.1186/s40623-018-0862-0>
- Nosé, M., Takahashi, K., Ohtani, S., Christon, S. P., & McEntire, R. W. (2005). Dynamics of ions of ionospheric origin during magnetic storms: Their acceleration mechanism and transport path to ring current. In T. I. Pulkkinen, N. A. Tsyganenko, & R. H. Friedel (Eds.), *The inner magnetosphere: Physics and modeling* (Geophys. Monogr. Ser., Vol. 155, pp. 61–71). <https://doi.org/10.1029/155gm08>

- O'Brien, T. P., & McPherron, R. L. (2000). An empirical phase space analysis of ring current dynamics: Solar wind control of injection and decay. *Journal of Geophysical Research*, 105(A4), 7707–7719. <https://doi.org/10.1029/1998JA000437>
- Sckopke, N. (1966). A general relation between the energy of trapped particles and the disturbance field near the Earth. *Journal of Geophysical Research*, 71, 3125–3130. <https://doi.org/10.1029/JZ0711013p03125>
- Sugiura, M. (1964). Hourly values of equatorial Dst for the IGY. *Annals of the International Geophysical Year*, 35, 9–45.
- Sugiura, M., & Chapman, S. (1960). *The average morphology of geomagnetic storms with sudden commencement* (Abhandl. Akad. Wiss. Goettingen Math. Physik. Kl. 4, pp. 51–53). [https://doi.org/10.1016/0038-092x\(60\)90024-4](https://doi.org/10.1016/0038-092x(60)90024-4)
- Sugiura, M., & Kamei, T. (1991). Equatorial Dst index 1957–1986, IAGA Bull. (Vol. 40). ISGI Pub. Office.
- Summers, D., Ni, B., & Meredith, N. P. (2007). Timescales for radiation belt electron acceleration and loss due to resonant wave-particle interactions: 2. Evaluation for VLF chorus, ELF hiss, and electromagnetic ion cyclotron waves. *Journal of Geophysical Research*, 112, A0427. <https://doi.org/10.1029/2006JA011993>
- Tsurutani, B. T., Gonzalez, W. D., Gonzalez, A. L. C., Guarnieri, F. L., Gopalswamy, N., Grande, M., et al. (2006). Corotating solar wind streams and recurrent geomagnetic activity: A review. *Journal of Geophysical Research*, 111, A07S01. <https://doi.org/10.1029/2005JA011273>
- Tsyganenko, N. A. (1982). Pitch-angle scattering of energetic particles in the current sheet of the magnetospheric tail and stationary distribution functions. *Planetary and Space Science*, 30(5), 433–437. [https://doi.org/10.1016/0032-0633\(82\)90052-6](https://doi.org/10.1016/0032-0633(82)90052-6)
- Tsyganenko, N. A., & Sitnov, M. I. (2005). Modeling the dynamics of the inner magnetosphere during strong geomagnetic storms. *Journal of Geophysical Research*, 110, A03208. <https://doi.org/10.1029/2004JA010798>
- Turner, N. E., Baker, D. N., Pulkkinen, T. I., & McPherron, R. L. (2000). Evaluation of the tail current contribution to Dst. *Journal of Geophysical Research*, 105(A3), 5431–5439. <https://doi.org/10.1029/1999JA000248>
- Wang, S.-Y., Kazama, Y., Jun, C.-W., Chang, T.-F., Hori, T., Miyoshi, Y., & Shinohara, I. (2018a). *The LEPE instrument level-2 3-D flux data of Exploration of energization and Radiation in Geospace (ERG) Arase satellite, Version v02\_02*. ERG Science Center, Institute for Space-Earth Environmental Research, Nagoya University. <https://doi.org/10.34515/DATA.ERG-04001>
- Wang, S.-Y., Kazama, Y., Jun, C.-W., Chang, T.-F., Hori, T., Miyoshi, Y., & Shinohara, I. (2018b). *The LEPE instrument level-2 omni-directional flux data of Exploration of energization and Radiation in Geospace (ERG) Arase satellite, Version v02\_02*. ERG Science Center, Institute for Space-Earth Environmental Research, Nagoya University. <https://doi.org/10.34515/DATA.ERG-04002>
- Weimer, D. R. (2005). Improved ionospheric electrodynamic models and application to calculating Joule heating rates. *Journal of Geophysical Research*, 110, A05306. <https://doi.org/10.1029/2004JA010884>
- Williams, D. J. (1981). Ring current composition and sources: An update. *Planetary and Space Science*, 29, 1195–1203. [https://doi.org/10.1016/0032-0633\(81\)90124-0](https://doi.org/10.1016/0032-0633(81)90124-0)
- Yokota, S., Kasahara, S., Hori, T., Keika, K., Miyoshi, Y., & Shinohara, I. (2018a). *The MEP-i instrument Level-2 3-D flux data of Exploration of energization and Radiation in Geospace (ERG) Arase satellite, Version v01\_01*. ERG Science Center, Institute for Space-Earth Environmental Research, Nagoya University. <https://doi.org/10.34515/DATA.ERG-03000>
- Yokota, S., Kasahara, S., Hori, T., Keika, K., Miyoshi, Y., & Shinohara, I. (2018b). *The MEP-i instrument Level-2 omni-directional flux data of Exploration of energization and Radiation in Geospace (ERG) Arase satellite, Version v01\_01*. ERG Science Center, Institute for Space-Earth Environmental Research, Nagoya University. <https://doi.org/10.34515/DATA.ERG-03001>
- Yokota, S., Kasahara, S., Mitani, T., Asamura, K., Hirahara, M., Takashima, T., et al. (2017). Medium-energy particle experiments—ion mass analyzer (MEP-i) onboard ERG (Arase). *Earth, Planets and Space*, 69(1), 172. <https://doi.org/10.1186/s40623-017-0754-8>
- Young, D. T., Balsiger, H., & Geiss, J. (1982). Correlations of magnetospheric ion composition with geomagnetic and solar activity. *Journal of Geophysical Research*, 87(A11), 9077–9096. <https://doi.org/10.1029/JA087iA11p09077>
- Young, S. L., Denton, R. E., Anderson, B. J., & Hudson, M. K. (2002). Empirical model for  $\mu$  scattering caused by field line curvature in a realistic magnetosphere. *Journal of Geophysical Research*, 107(A6). <https://doi.org/10.1029/2000JA000294>
- Young, S. L., Denton, R. E., Anderson, B. J., & Hudson, M. K. (2008). Magnetic field line curvature induced pitch angle diffusion in the inner magnetosphere. *Journal of Geophysical Research*, 113, A03210. <https://doi.org/10.1029/2006JA012133>
- Yu, Y., Jordanova, V., Zaharia, S., Koller, J., Zhang, J., & Kistler, L. M. (2012). Validation study of the magnetically self-consistent inner magnetosphere model RAM-SCB. *Journal of Geophysical Research*, 117, A03222. <https://doi.org/10.1029/2011JA017321>
- Yu, Y., Jordanova, V. K., Ridley, A. J., Toth, G., & Heelis, R. (2017). Effects of electric field methods on modeling the midlatitude ionospheric electrodynamics and inner magnetosphere dynamics. *Journal of Geophysical Research: Space Physics*, 122, 5321–5338. <https://doi.org/10.1002/2016ja023850>
- Yu, Y., Ridley, A. J., Welling, D. T., & Tóth, G. (2010). Including gap region field-aligned currents and magnetospheric currents in the MHD calculation of ground-based magnetic field perturbations. *Journal of Geophysical Research*, 115, A08207. <https://doi.org/10.1029/2009JA014869>
- Yu, Y., Tian, X., & Jordanova, V. K. (2020). The effects of field line curvature (FLC) scattering on ring current dynamics and isotropic boundary. *Journal of Geophysical Research: Space Physics*, 125, e2020JA027830. <https://doi.org/10.1029/2020JA027830>
- Yue, C., Zong, Q., Wang, Y., Vogiatzis, I. I., Pu, Z., Fu, S., & Shi, Q. (2011). Inner magnetosphere plasma characteristics in response to interplanetary shock impacts. *Journal of Geophysical Research*, 116, A11206. <https://doi.org/10.1029/2011JA016736>
- Zaharia, S., Cheng, C., & Maezawa, K. (2004). 3-D force-balanced magnetospheric configurations. *Annales Geophysicae*, 22, 251–265. <https://doi.org/10.5194/angeo-22-251-2004>
- Zaharia, S., Jordanova, V. K., Thomsen, M. F., & Reeves, G. D. (2006). Self-consistent modeling of magnetic fields and plasmas in the inner magnetosphere: Application to a geomagnetic storm. *Journal of Geophysical Research*, 111, A11S14. <https://doi.org/10.1029/2006JA011619>
- Zhao, H., Li, X., Baker, D. N., Claudepierre, S. G., Fennell, J. F., Blake, J. B., et al. (2016). Ring current electron dynamics during geomagnetic storms based on the Van Allen Probes measurements. *Journal of Geophysical Research: Space Physics*, 121, 3333–3346. <https://doi.org/10.1002/2016JA022358>
- Zhao, H., Zhao, H., Li, X., Baker, D. N., Fennell, J. F., Blake, J. B., et al. (2015). The evolution of ring current ion energy density and energy content during geomagnetic storms based on Van Allen Probes measurements. *Journal of Geophysical Research: Space Physics*, 120, 7493–7511. <https://doi.org/10.1002/2015JA021533>